Electronic Supporting Information for

Iron(II) Spin Crossover Complexes of Tetradentate Schiff-Bases: Tuning $T_{1/2}$ by Choice of Formyl-heterocycle Component

Matthew G. Robb,[a] Shen Chong,[b] and Sally Brooker[a]*

[a] *Department of Chemistry and MacDiarmid Institute of Advanced Materials and Nanotechnology, University of Otago, P.O. Box 56, Dunedin 9054, New Zealand. Email: sbrooker@chemistry.otago.ac.nz*

[b] *Robinson Research Institute, Victoria University Wellington, PO Box 33436, Lower Hutt 5046, New Zealand.*

Contents

S1. Crystallographic Data

S1.1. Data Tables

*Table S1: Selected crystallographic data for the mononuclear complexes [Fe(**L**^{4thiazole})(NCS)$_2$] (**1**), [Fe(**L**^{2thiazole})(NCS)$_2$] (**2**) and [Fe(**L**^{oxazole})(NCS)$_2$] (**3**) at 100 K.*

	[Fe(**L**^{4thiazole})(NCS)$_2$] (**1**)	[Fe(**L**^{2thiazole})(NCS)$_2$] (**2**)	[Fe(**L**^{4oxazole})(NCS)$_2$] (**3**)
Identification code	MGR397	MGR421	MGR412
Empirical formula	$C_{13}H_{12}FeN_6S_4$	$C_{13}H_{12}FeN_6S_4$	$C_{13}H_{12}FeN_6O_2S_2$
Formula weight	436.38	436.38	404.26
Temperature/K	100.00(10)	100.01(10)	100
Crystal system	monoclinic	monoclinic	monoclinic
Space group	$P2_1/c$	$P2_1/c$	$P2_1/n$
a/Å	8.1875(2)	8.4981(3)	8.07340(10)
b/Å	25.0403(5)	22.9024(8)	8.1467(2)
c/Å	8.7689(2)	9.2014(3)	25.2676(5)
α/°	90	90	90
β/°	91.862(2)	93.712(3)	94.860(2)
γ/°	90	90	90
Volume/Å^3	1796.83(7)	1787.08(11)	1655.91(6)
Z	4	4	4
ρ_{calc}g/cm^3	1.613	1.622	1.622
μ/mm^{-1}	11.152	11.213	9.847
F(000)	888	888	824
Crystal size/mm^3	0.138 × 0.094 × 0.046	0.209 × 0.1 × 0.069	0.586 × 0.247 × 0.117
Radiation	Cu Kα (λ = 1.54184)	Cu Kα (λ = 1.54184)	CuKα (λ = 1.54184)
2Ө range for data collection/°	10.694 to 145.18	7.72 to 145.28	7.022 to 145.364
Index ranges	-9 ≤ h ≤ 10, -28 ≤ k ≤ 30, -10 ≤ l ≤ 10	-10 ≤ h ≤ 10, -27 ≤ k ≤ 19, -11 ≤ l ≤ 11	-9 ≤ h ≤ 9, -10 ≤ k ≤ 10, -30 ≤ l ≤ 30
Reflections collected	10087	13089	12392
Independent reflections	3501 [R_{int} = 0.0304, R_{sigma} = 0.0323]	3479 [R_{int} = 0.0480, R_{sigma} = 0.0444]	3235 [R_{int} = 0.0534, R_{sigma} = 0.0417]
Data/restraints/parameters	3501/0/217	3479/0/217	3235/0/217
Goodness-of-fit on F^2	1.021	1.067	1.024
Final R indexes [I>=2σ (I)]	R_1 = 0.0292, wR_2 = 0.0701	R_1 = 0.0517, wR_2 = 0.1249	R_1 = 0.0393, wR_2 = 0.1008
Final R indexes [all data]	R_1 = 0.0359, wR_2 = 0.0734	R_1 = 0.0740, wR_2 = 0.1382	R_1 = 0.0473, wR_2 = 0.1068
Largest diff. peak/hole / e Å^{-3}	0.72/-0.42	0.84/-0.37	0.90/-0.35

*Table S2: Selected crystallographic data for the polymorph I of [Fe(**L$^{5Br-pyridine}$**)(NCS)$_2$] (**4A**) at 100 K and 280 K, and polymorph II of [Fe(**L$^{5Br-pyridine}$**)(NCS)$_2$] (**4B**) at 100 K.*

	[Fe(**L$^{5Br-pyridine}$**)(NCS)$_2$] (**4A**) Polymorph I	[Fe(**L$^{5Br-pyridine}$**)(NCS)$_2$] (**4A**) Polymorph I	[Fe(**L$^{5Br-pyridine}$**)(NCS)$_2$] (**4B**) Polymorph II
Identification code	MGR464	MGR496_280K_auto	MGR464_2_auto
Empirical formula	C$_{17}$H$_{14}$Br$_2$FeN$_6$S$_2$	C$_{17}$H$_{14}$Br$_2$FeN$_6$S$_2$	C$_{17}$H$_{14}$Br$_2$FeN$_6$S$_2$
Formula weight	582.13	582.13	582.13
Temperature/K	100	279.99(11)	100
Crystal system	monoclinic	monoclinic	triclinic
Space group	P2$_1$/n	P2$_1$	P-1
a/Å	8.6122(2)	9.0297(4)	8.3520(4)
b/Å	24.3739(4)	24.7207(10)	11.5772(5)
c/Å	10.6495(2)	10.4302(4)	11.6323(4)
α/°	90	90	72.401(4)
β/°	111.055(3)	111.078(5)	88.978(4)
γ/°	90	90	85.259(4)
Volume/Å^3	2086.22(8)	2172.46(17)	1068.42(8)
Z	4	4	2
ρ$_{calc}$g/cm^3	1.853	1.78	1.81
μ/mm^{-1}	12.293	11.805	12.002
F(000)	1144	1144	572
Crystal size/mm^3	0.184 × 0.056 × 0.043	0.234 × 0.078 × 0.042	0.354 × 0.12 × 0.069
Radiation	CuKα (λ = 1.54184)	Cu Kα (λ = 1.54184)	CuKα (λ = 1.54184)
2Θ range for data collection/°	7.254 to 149.294	7.152 to 145.344	7.974 to 149.314
Index ranges	-10 ≤ h ≤ 10, -30 ≤ k ≤ 28, -12 ≤ l ≤ 13	-11 ≤ h ≤ 7, -30 ≤ k ≤ 29, -7 ≤ l ≤ 12	-7 ≤ h ≤ 7, -14 ≤ k ≤ 14, -14 ≤ l ≤ 12
Reflections collected	15957	8949	14063
Independent reflections	4209 [R$_{int}$ = 0.0437, R$_{sigma}$ = 0.0320]	6336 [R$_{int}$ = 0.0482, R$_{sigma}$ = 0.0674]	3740 [R$_{int}$ = 0.0806, R$_{sigma}$ = 0.0546]
Data/restraints/parameters	4209/0/253	6336/7/506	3740/0/267
Goodness-of-fit on F^2	1.054	1.038	1.041
Final R indexes [I>=2σ (I)]	R$_1$ = 0.0353, wR$_2$ = 0.0914	R$_1$ = 0.0772, wR$_2$ = 0.1952	R$_1$ = 0.0640, wR$_2$ = 0.1759
Final R indexes [all data]	R$_1$ = 0.0378, wR$_2$ = 0.0938	R$_1$ = 0.0862, wR$_2$ = 0.2147	R$_1$ = 0.0729, wR$_2$ = 0.1890
Largest diff. peak/hole / e Å^{-3}	0.70/-0.56	2.68/-0.76	2.31/-1.01
Flack parameter	-	0.495(13)	-

S1.2. Packing Interactions

S1.2.1 [Fe(L^{4thiazole})(NCS)$_2$] (1)

The asymmetric unit of **1** consists of one [Fe(**L^{4thiazole}**)(NCS)$_2$] complex (Figure S1).

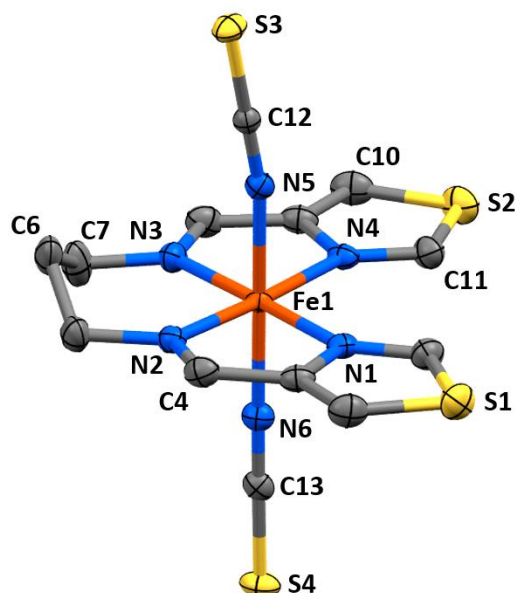*Figure S1: Asymmetric unit of **1**.*

The structure of **1** features 1D chains of complex, formed through CH···S interactions involving S3 and H11 on adjacent molecules (C11···S3 distance = 3.500(3) Å), which run along the *a* axis in the lattice (Figure S2, a, pink line to guide the eye). A short intermolecular S···S contact is also noted along this chain (3.5690(8) Å). The chains are linked into two dimensional sheets through a number of CH···S interactions between symmetry related, adjacent, complexes (Figure S2, b, orange line to guide the eye towards the 2D sheets). Short contacts are observed between C10-H10···S4 (C···S distance = 3.637(3) Å), C8-H8···C12 (C8···C12 distance = 3.598(3) Å), and C7-H7a···S3 (3.694(3) Å).

A 3D framework is constructed through a number of short contacts between the previously described 2D layers, including a non-classical interaction between C4 and S4 of an adjacent thiocyanate ligand (C4···S4 distance = 3.7042 Å) and an interaction between the thiazole S and adjacent thiocyanate ligand (S1···S3 = 3.4954(7) Å, S1···C12 = 3.485(2) Å). and S···S interactions (Figure S2, c, orange lines to guide the eye towards the 2D sheets described previously). Also running through the lattice, along the ac-axis, is a 1D chain of complexes formed through non-classical H-bonding interactions between S2(thiazole) and the hydrogen atoms on C6 and C7 (C6···S2 = 3.682(3) Å, C7···S2 = 3.602(3) Å, Figure S2, e).

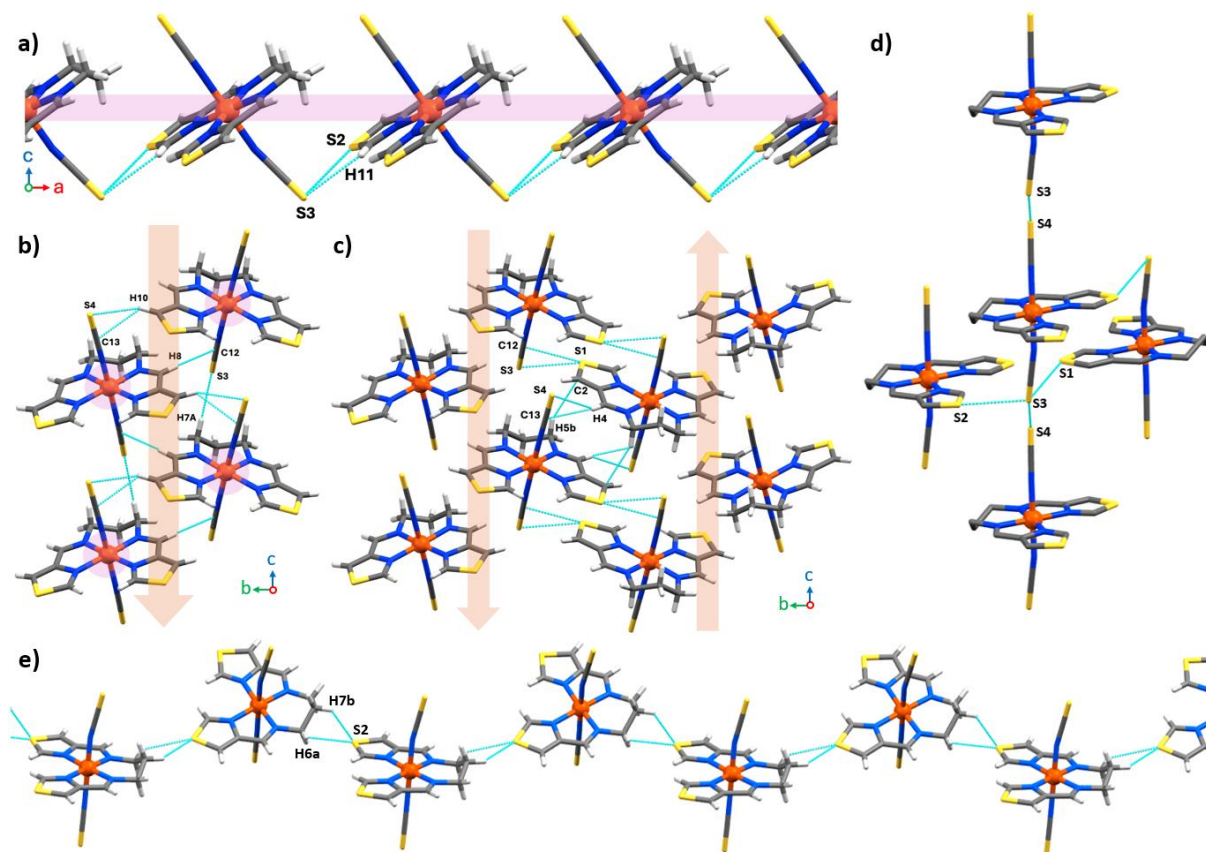*Figure S2: Selected intermolecular interactions and packing in [Fe(L^4thiazole)(NCS)₂] (1) at 100 K. a) Formation of 1D chains of complex (pink line to guide the eye) of 1 formed along the a-axis through the interaction of C11···S3. b) Interactions (blue dotted line) between molecules of 1 linking the 1D chains into 2D sheets. c) Interactions between the 2D sheets that lead to the formation of a 3D short contact network in 1. d) Short intermolecular S···S contacts between neighbouring molecules in the structure of 1. e) Perspective view of the 1D chain formed (ac-axis) through interactions of the thiazole S2 and the backbone CH of neighbouring complexes.*

Table S3: Selected intermolecular contacts in the structure of 1, [Fe(L^4thiazole)(NCS)₂], at 100 K. Non-classical C-H ···Donor hydrogen bonds in black text; C-H ···π(NCS) in blue text. All H atoms were inserted at calculated positions and rode on the attached non-H atom, with temperature factors U(H) = 1.2 U.

D-H···A	H···A / Å	D···A / Å	D-H···A / °	Symm. Op. for Acceptor	Figure
C4 – H4 ··· S4(NCS)	2.8700	3.704(2)	150.0	1-x,1-y,1-z	Fig. S2c
C10 – H10 ··· S4(NCS)	2.8000	3.637(3)	150.0	x,3/2-y,-1/2+z	Fig. S2b
C10 – H10 ··· C13(NCS)	2.8700	3.531(3)	129.0		
C11 – H11 ··· S3(NCS)	2.9100	3.500(3)	123.0	-1+x,y,z	Fig. S2a
C7 – H7a ··· S3(NCS)	2.8900	3.694(3)	140.0	x,y,1+z	Fig. S2b
C8 – H8 ··· C12(NCS-3)	2.6800	3.598(3)	169.0	x,3/2-y,1/2+z	Fig. S2b
C8 – H8 ··· N5(NCS-3)	2.9400	3.84	166.0		
C6 – H6A ··· S2(thiazole)	2.9900	3.682(3)	129.0	1+x,3/2-y,1/2+z	Fig. S2e
C7 – H7B ··· S2(thiazole)	2.9300	3.602(3)	128.0	1+x,3/2-y,1/2+z	Fig. S2e
S3(NCS) ··· S1(thiazole)		3.4954(7)		1-x,1-y,-z	Fig. S2d
S3(NCS) ··· S2(thiazole)		3.5690(8)		1+x,y,z	Fig S2a&d
S3(NCS) ··· S4(NCS)		3.5813(7)		1+x,y,-1+z	Fig. S2d

S1.2.2 [Fe(L$^{\text{2thiazole}}$)(NCS)$_2$] (2)

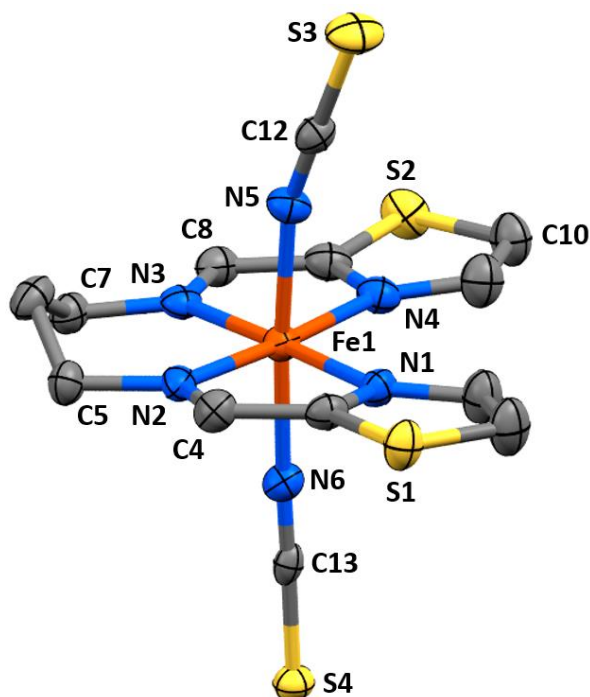The asymmetric unit of **2** consists of one [Fe(**L**$^{\text{2thiazole}}$)(NCS)$_2$] complex (Figure S3).

*Figure S3: Asymmetric unit of **2**.*

The crystal packing interaction is **2** are dominated by short C-H···S contacts between the thiocyanate co-ligands and neighbouring molecules, along with some short S···S contacts. The formation of a 1D supramolecular ladder along the crystallographic *c*-axis is supported by intermolecular short contacts between C10-H10···S4 (C ··· S distance = 3.477(5) Å), S2···S4 (S ··· S distance = 3.4060(18) Å) and C7-H7B···S4 (C ··· S distance = 3.641(5) Å) (Figure S4, a, highlighted by orange line). Neighbouring supramolecular 'ladders' are connected along the *b*-axis to form 2D supramolecular sheets through a number of interactions (Figure S, c). Two C-H···S interactions are involved; C4-H4···S4 (C ··· S distance = 3.621(5) Å) and C5-H5b···S1 (C ··· S distance = 3.748(5) Å), long with one short intermolecular S···S contact; S1···S4 (S ··· S distance = 3.4895(18) Å). The 2D sheets are connected into a 3D lattice through short contacts between C8-H8···S3 (C ··· S distance = 3.833 Å) and S1···S4 (3.4895(16) Å) along the *b*-axis (Figure S4, b).
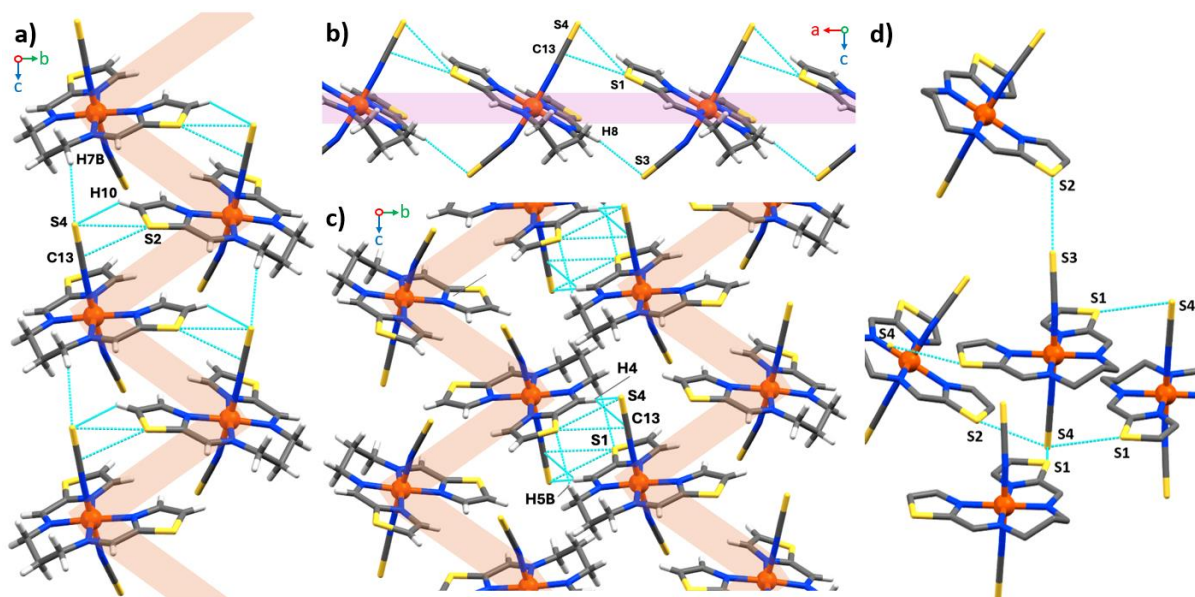
*Figure S4: Selected intermolecular interactions and packing in [Fe($L^{2thiazole}$)(NCS)$_2$] (**2**) at 100 K. a) Formation of 1D ladder-chains of complex (orange line to guide the eye) of **2** formed along the c-axis. b) Interactions (blue dotted line) between the previously defined 'ladders' of **2** linking the 1D chains into 2D sheets along the ac-plane. c) Interactions between the 2D sheets that lead to the formation of a 3D short contact network in **2**.*

*Table S4: Selected intermolecular contacts in the structure of **2** at 100 K. All H atoms were inserted at calculated positions and rode on the attached non-H atom, with temperature factors U(H) = 1.2 U.*

D-H···A	H···A / Å	D···A / Å	D-H···A / °	Symm. Op. For Acceptor	Figure
C4 – H4 ··· S4(NCS)	2.860	3.621(5)	138.0	1-x,1-y,1-z	Fig. S4c
C7 – H7B ··· S4(NCS)	2.840	3.641(5)	139.0	x,y,1+z	Fig. S4a
C7 – H7A ··· S4(NCS)	2.890	3.641(5)	144.0	x,y,1+z	Fig. S4c
C10 – H10 ··· S4(NCS)	2.990	3.477(5)	114.0	x,3/2-y,1/2+z	Fig. S4a
C8 – H8 ··· S3(NCS)	2.920	3.833(5)	169.0	-1+x,y,z	Fig. S4b
C5 – H5B ··· S1(thiazole)	2.860	3.748(5)	150.0	1-x,1-y,1-z	Fig. S4c
S4(NCS) ··· S1(thiazole)		3.4895(16)		-1+x,y,z	Fig. S4d
S2(thiazole) ··· S3(NCS)		3.5920(18)		-1+x,3/2-y,-1/2+z	Fig. S4d
S2(thiazole) ··· S4(NCS)		3.4060(18)		x,3/2-y,1/2+z	Fig. S4d

S1.2.3 [Fe(L^{4oxazole})(NCS)$_2$] (3)

The asymmetric unit of **3** consists of one [Fe(L^{4oxazole})(NCS)$_2$] complex (Figure S5). The central carbon atom (C6) of the propylene fragment is disordered over two positions, up and down, 85/15.
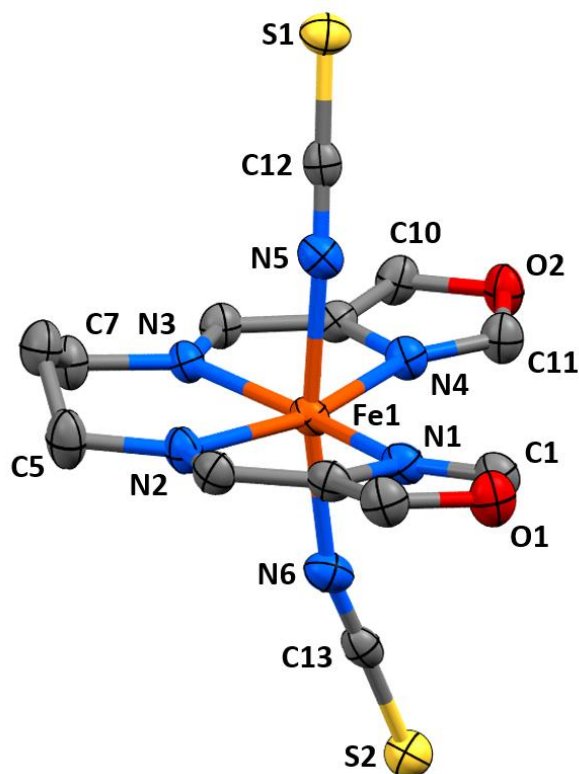

*Figure S5: Asymmetric unit of **3**, showing the major disorder component (85%) of the central carbon atom (C6) of the propylene chain.*

Notable in **3** is the formation of dimers of the complex through reciprocated hydrogen bonds between H1 and H11 of one complex with one of the thiocyanates on the paired complex (S1 and C12 (C1···S1 distance 3.541(3) Å, C11···S1 distance 3.742 Å) (Fig S6, a). Non-classical hydrogen bonds between adjacent 4-oxazole rings, namely mutual C11-H···O2 pairs (C11···O2 3.170(4) Å), combined with the interactions that lead to the previously described dimer formation, form 1D chains of complexes along the *a*-axis (Figure S6, b). The non-classical hydrogen bonding between C7-H7b and S2 (C ··· S distance 3.704 Å) lead to the formation of 2D sheets of complex. This leads to short contacts between S2 and the ligand of adjacent molecules (C8, C9 and C10). Also involved in the stabilisation of the 2D sheet along the *ab*-plane is a non-classical hydrogen bond C10-H10 ··· O1 (C10 ··· O1 distance 3.607 Å, Fig S6, d)).

The 2D sheets are connected through a series of non-classical H-bonds involving the thiocyanate coligand and the alkyl backbone of neighbouring complexes (Fig S6, major disorder component shown in e, minor component in f).
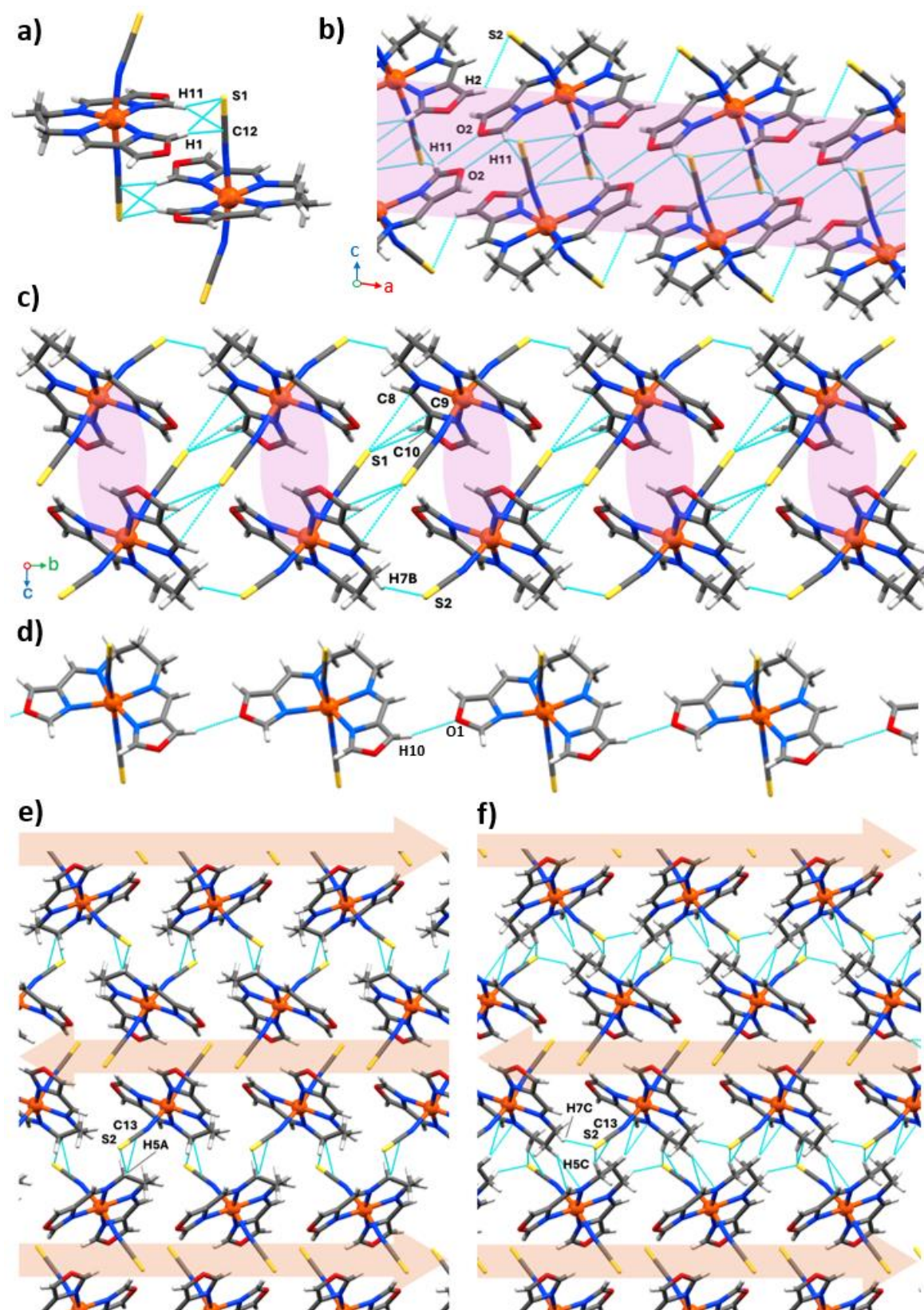
*Figure S6: a) Perspective view of the formation of dimers of complex [Fe(**L**^{4oxazole})(NCS)₂] **3**. b) View down the b-axis highlighting the formation of supramolecular 1D chains of complex along the a-axis. c) View down the a-axis showing the connections between the previously described 1D chains, that leads to the formation of 2D sheets. d) Perspective view of the C10-H10···O1 non-classical interaction that runs along the ab-axis. e) Interactions between the previously defined sheets. the major part of the disorder of the propyl fragment (85%) is shown. f) Interactions between the previously defined sheets. the minor part of the disorder of the propyl fragment (15%) is shown.*

*Table S5: Selected intermolecular contacts in the structure of **3** at 100 K. Note that interactions from the diaminopropane moiety are from the main disorder components (where occupancy is 85%). All H atoms were inserted at calculated positions and rode on the attached non-H atom, with temperature factors U(H) = 1.2 U.*

D-H⋯A	H⋯A / Å	D⋯A / Å	D-H⋯A / °	Symm. Op for A	Figure
C11 - H11 ⋯ O2(oxazole)	2.700	3.170(4)	112.0	-x,1-y,1-z	Fig. S6b
C10 – H10 ⋯ O1(oxazole)	2.700	3.607(4)	166.4	-1+x,1+y,z	Fig. S6d
C1 - H1 ⋯ S1(NCS)	2.770	3.641(3)	157.0	x,-1+y,z	Fig. S6a
C11 - H11 ⋯ S1(NCS)	2.880	3.742(3)	155.0	1-x,1-y,1-z	Fig. S6a
C2 – H2 ⋯ S2(NCS)	2.960	3.583(3)	125.0	1+x,y,z	Fig. S6b
C5 – H5a ⋯ S2(NCS)	2.930	3.779(3)	146.0	3/2-x,1/2+y,3/2-z	Fig. S6e
C5 – H5c ⋯ S2(NCS)	2.998	3.779(3)	139	3/2-x,1/2+y,3/2-z	Fig. S6f
C7-H7c ⋯ S2(NCS)	2.936	3.822(3)	152	x,1+y,z	Fig. S6f

S1.2.4 [Fe(L$^{5Br\text{-pyridine}}$)(NCS)$_2$] Polymorph A (4A)

The asymmetric unit of **4A** consists of one [Fe(**L$^{5Br\text{-pyridine}}$**)(NCS)$_2$] complex (Figure S7Figure S5).

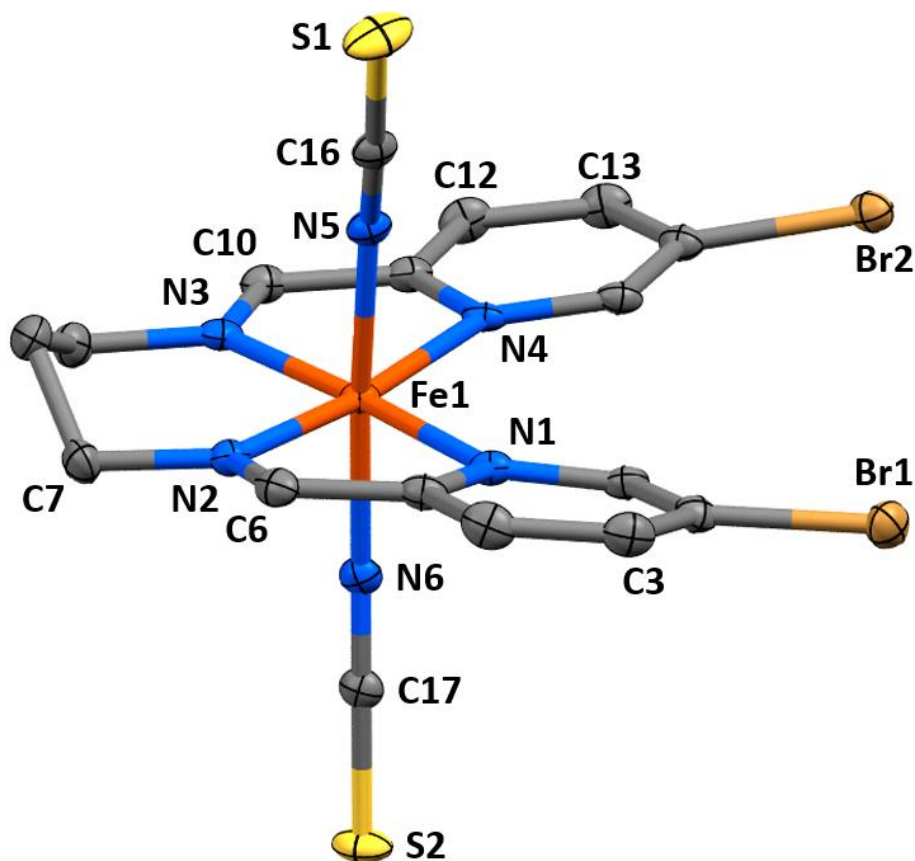*Figure S7: Asymmetric unit of **4A** at 100 K.*

Looking at **4A** the complexes form 1D chains along the *a*-axis through C-H⋯S interactions involving S1 and H10 (C10 ⋯ S1 distance = 3.837), and interactions between the ligand H3 and the C≡N of the thiocyanate (C3 ⋯ C17 distance = 3.321(5)) (Figure S8, a, pink lines to guide the eye). These chains are connected into a 2D sheet spanning the *ac*-plane through hydrogen bond interactions between Br1 and H7a and H7b (C7 ⋯ Br1 distance = 3.260(3) Å) (Figure S8, a).

The 2D sheets are linked through a number of intermolecular contacts involving the thiocyanate co-ligand and adjacent complexes (Figure S8, b and c). Included in this are interactions between Br2 with S1 and S2 (Br2 ⋯ S1 distance = 3.5756(11), Br1 ⋯ S2 distance = 3.5228(9) Å), a C - H ⋯ S contacts involving the thiocyanate co-ligand; C6-H6 ⋯ S2 (distance = 3.766(3) Å), and interactions between the C≡N and adjacent hydrogen atoms; C12 – H12 ⋯ C16 (C ⋯ C distance 3.368(5) Å) and C13 – H13 ⋯ C16 (C ⋯ C distance 3.271(5) Å).
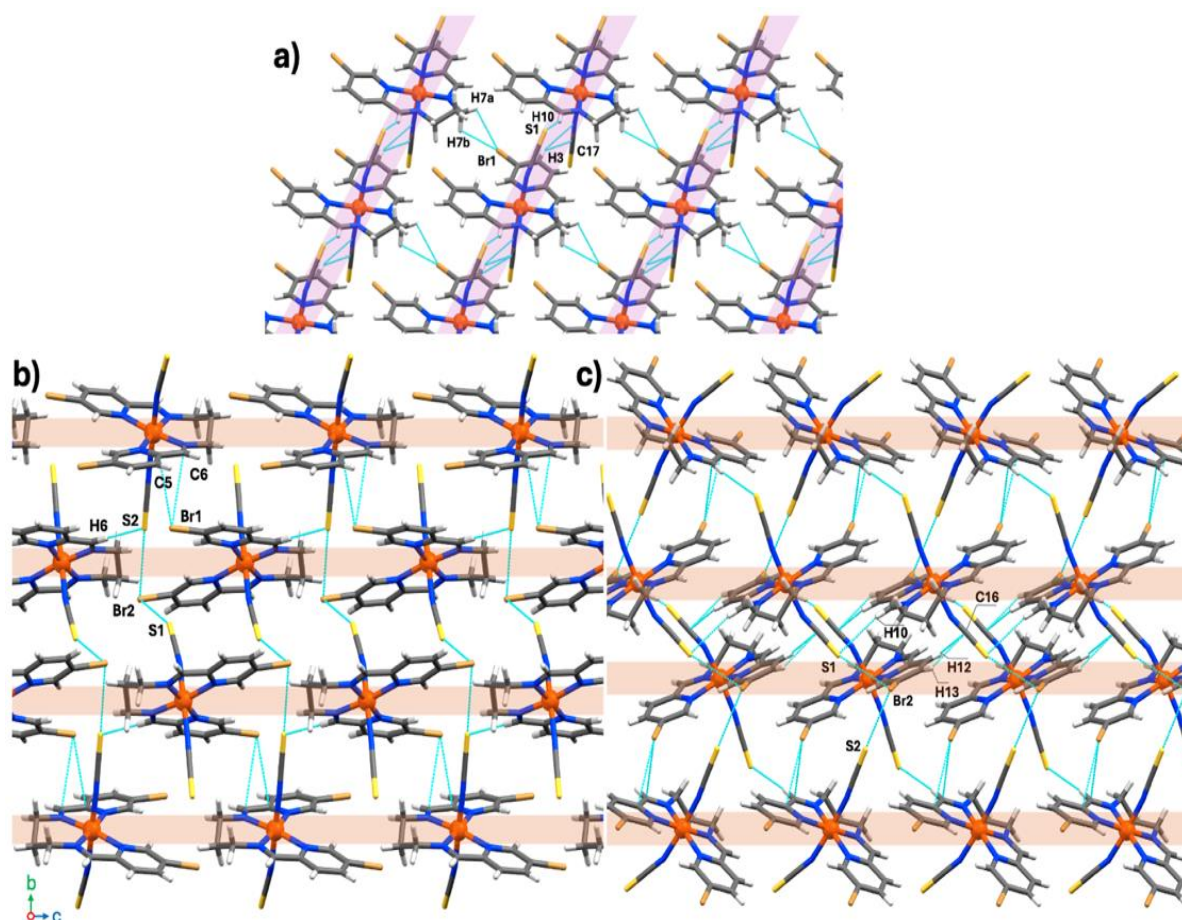
*Figure S8: Packing interactions in polymorph A of [Fe($L^{5Br-pyridine}$)(NCS)$_2$] **4A** at 100 K. a) Perspective view of the 2D sheets formed along the ac-plane, pink link to highlight the chains along the a-axis. B) View along the a-axis, highlighting the interactions between the previously described sheets, orange lines to highlight the 2D sheets along the ac-plane. C) View along the c-axis, highlighting the interactions between the previously described sheets, orange lines to highlight the 2D sheets along the ac-plane.*

*Table S6: Selected intermolecular contacts in the structure of **4A** at 100 K. Non-classical C-H ···Donor hydrogen bonds in black text; C-H ···π(NCS) in blue text. All H atoms were inserted at calculated positions and rode on the attached non-H atom, with temperature factors U(H) = 1.2 U.*

D-H···A	H···A / Å	D···A / Å	D-H···A / °	Symm. Op for A	Figure
C6 - H6 ··· S2(NCS)	2.850	3.766(3)	170.0	-1/2+x,3/2-y,1/2+z	Fig. S8b
C10 - H10 ··· S1(NCS)	2.960	3.837(3)	158.0	1+x,y,z	Fig. S8a
C3 – H3 ··· C17(NCS)	2.520	3.321(5)	144.0	1+x,y,z	Fig. S8a
C3 – H3 ··· N6(NCS)	2.690	3.485(5)	142.0		
C12 – H12 ··· C16(NCS)	2.840	3.368(5)	117.0	2-x,1-y,1-z-	Fig. S8c
C12 – H12 ··· N5(NCS)	2.980	3.367(4)	106.0		
C13 – H13 ··· C16(NCS)	2.660	3.271(5)	124.0	2-x,1-y,1-z	Fig. S8c
C13 – H13 ··· C5(NCS)	2.760	3.235(4)	112.0		
C7 - H7A ··· Br1	2.900	3.260(3)	103.0	1+x,y,1+z	Fig. S8a
C7 - H7B ··· Br1	2.910	3.260(3)	102.0	1+x,y,1+z	Fig. S8a
Br3 ··· S2(NCS)		3.5228(9)		1-x,1-y,1-z	Fig. S8b
Br2 ··· S1(NCS)		3.5756(11)		1-x,1-y,1-z	Fig. S8b

As noted above, heating crystals of polymorph **4A** to 280 K leads to a symmetry-breaking phase transition and two unique complexes in the asymmetric unit, both in the HS state (Figure S9). Due to this the packing of the complex is modified slightly. Notable is the lengthening (and in some case breaking) of intermolecular contacts.
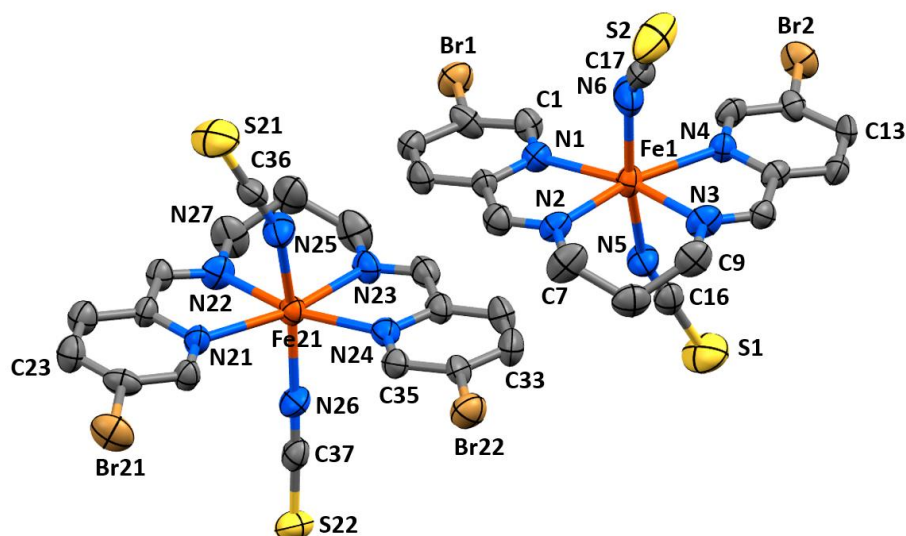

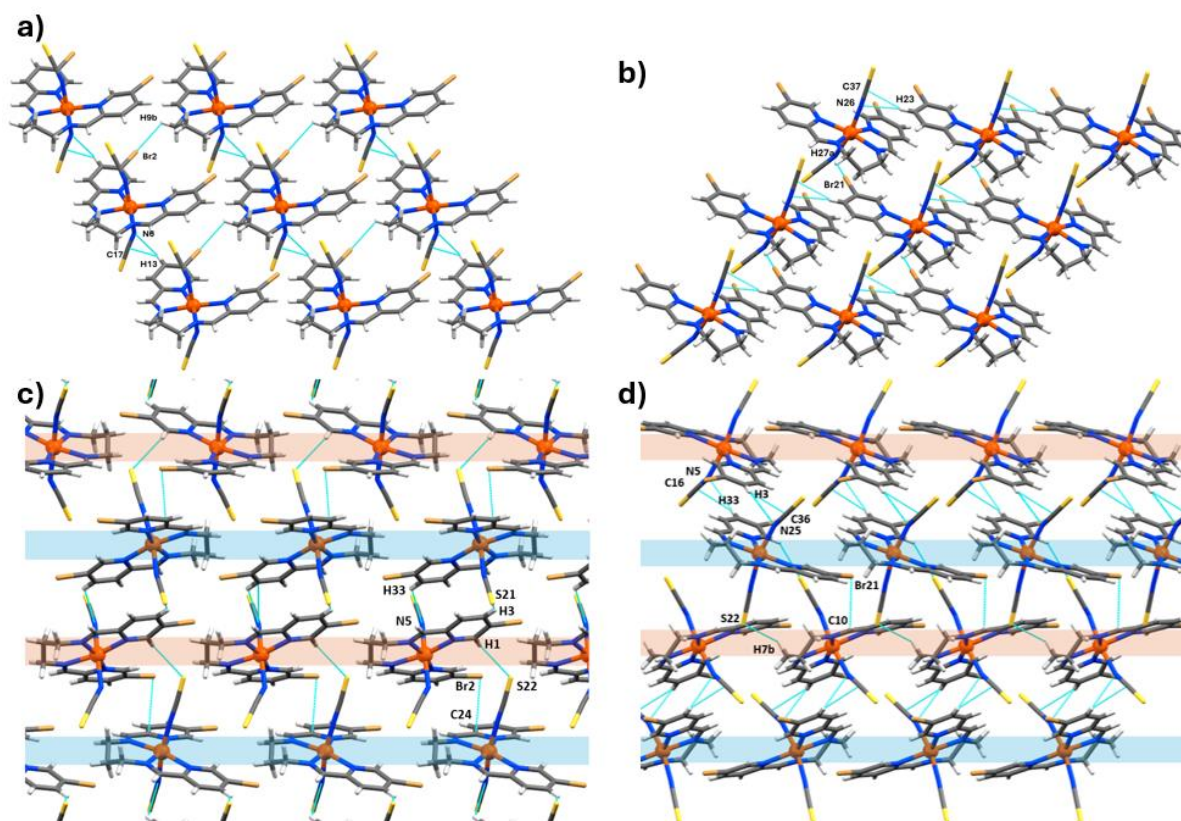*Figure S9: Asymmetric unit of **4A** at 280 K contains two full molecules, Fe(1) and Fe(21).*

*Figure S10: Packing interactions in polymorph A of [Fe(L^{5Br-pyridine})(NCS)₂] **4A** at 280 K. a) Perspective view of the 2D sheets of the first complex in the asymmetric unit formed along the ac-plane. b) Perspective view of the 2D sheets of the second complex in the asymmetric unit formed along the ac-plane. c) View along the a-axis, highlighting the interactions between the previously described sheets, orange and blue lines to highlight the 2D sheets of the first complex and second complex respectively, along the ac-plane. d) View along the c-axis, highlighting the interactions between the previously described sheets, and blue lines to highlight the 2D sheets of the first complex and second complex respectively.*

*Table S7: Selected intermolecular contacts in the structure of polymorph A of [Fe(**L^{5Br-pyridine}**)(NCS)₂] **4A** at 280 K. Non-classical C-H ···Donor hydrogen bonds in black text; C-H ···π(NCS) in blue text. All H atoms were inserted at calculated positions and rode on the attached non-H atom, with temperature factors U(H) = 1.2 U.*

| D-H···A	H···A / Å	D···A / Å	D-H···A / °	Symm. Op for A	Figure
D from either molecule, but A from 1st molecule (Fe1) in asymmetric unit					
C9 - H9a ··· Br2	3.100	3.340(15)	96.0	1+x,y,1+z	Fig. S10a
C9 - H9b ··· Br2	2.830	3.340(15)	114.0	1+x,y,1+z	Fig. S10a
C13 – H13 ··· N6(NCS-2)	2.610	3.51(3)	163.0	1+x,y,z	Fig. S10a
C13 – H13 ··· C17(NCS-2)	2.610	3.47(3)	150,0		Fig. S10a
C33 – H33 ··· N5(NCS-1)	2.660	3.25(2)	122.0	N/A: D is from 2nd molecule in asym. unit	Fig. S10d
C33 – H33 ··· C16(NCS-1)	2.760	3.43(3)	130.0		Fig. S10c&d
C35 – H35 ··· S2(NCS)	2.9200	3.646(18)	135.0	N/A: D is from 2nd molecule in asym. unit	Not shown
D from either molecule, but A from 2ⁿᵈ molecule (Fe21) in asymmetric unit					
D-H···A	**H···A / Å**	**D···A / Å**	**D-H···A / °**	**Symm. Op for A**	**Figure**
C27 – H27a ··· Br21	2.900	3.479(18)	119.0	x,y,1+z	Fig. S10b
C10 – H10 ··· Br21	3.240	3.516(13)	100.0	-x, 1/2+y, -z	Fig. S10d
C23 – H23··· N26(NCS-22)	2.640	3.56(3)	169.0	-1+x,y,z	Fig S10b
C23 – H23 ··· C37(NCS-22)	2.600	3.51(3)	163.0		Fig S10b
C3 – H3 ··· N25(NCS-21)	2.650	3.24(3)	121.0		Fig S10d
C3 – H3 ··· C36(NCS-21)	2.770	3.43(3)	129.0		Fig S10d
C1 – H1 ··· S22(NCS)	2.890	3.689(18)	143.0	1-x,1/2+y,1-z	Fig S10c
C7 – H7b ··· S22(NCS)	2.920	3.705	136.0	-x,1/2+y,-z	FigS10d
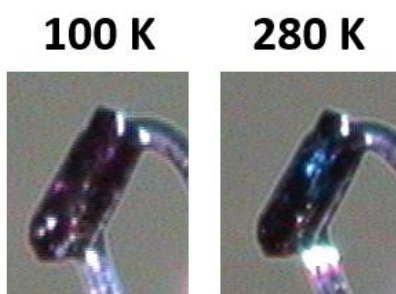
*Figure S11: Photos of a single crystal of **4A** at 100 K (left, purple) and 280 K (right, blue).*

S1.2.5 [Fe(L^{5Br-pyridine})(NCS)₂] Polymorph B (4B)

S1.2.5 $[Fe(L^{5Br\text{-}pyridine})(NCS)_2]$ Polymorph B (4B)

The asymmetric unit of **4B** consists of one $[Fe(\mathbf{L^{5Br\text{-}pyridine}})(NCS)_2]$ complex (Figure S12).
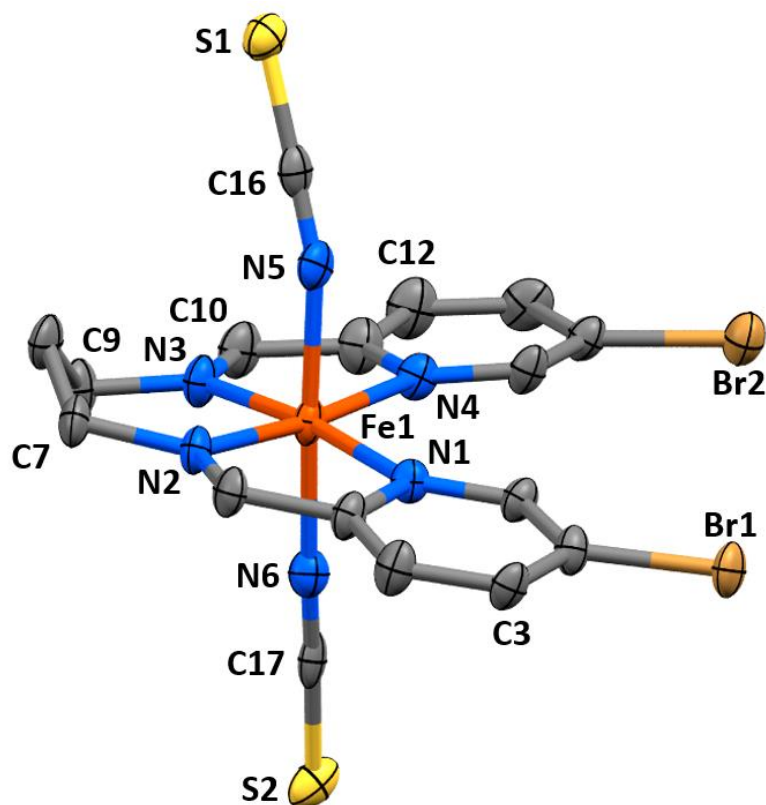

*Figure S12: Asymmetric unit of **4B** at 100 K.*

In contrast to **4A**, polymorph **4B** (100 K) does not feature any C-H···Br interactions. Instead, the crystal packing is dominated by non-classical hydrogen bonding contacts between the S atoms of the thiocyanate ligands and the hydrogen atoms from the adjacent complex (Figure S13, a), and some short intermolecular S···Br contact. The complexes form a 1D chain along the crystallographic *a*-axis through a CH···S non-classical hydrogen bond between H12 and an adjacent thiocyanate co-ligand (C12 ··· S2 distance = 3.613(8) Å, Figure S13, a). This leads to a short Br1 ··· Br2 distance of 3.6922(10) Å.

The chains are linked together through other C - H ··· S interactions involving the thiocyanate, as well as a S ··· Br interaction (Figure S13, b). Pairs of chains are linked together through mutual short interactions between Br1 ··· S2 (distance =3 .4278(19) Å) on adjacent complexes. The 'pairs of chains' are linked together through interactions nonclassical C-H interactions with thiocyanate ligands on adjacent complexes; C3 - H3 ··· C16 (C3 ··· C16 distance = 3.441(9) Å), C10-H10 ··· S2 (C10 ··· S2 distance = 3.612(7) Å), C9-H9a ··· S2 (C9 ··· S2 distance = 3.441(9) Å).

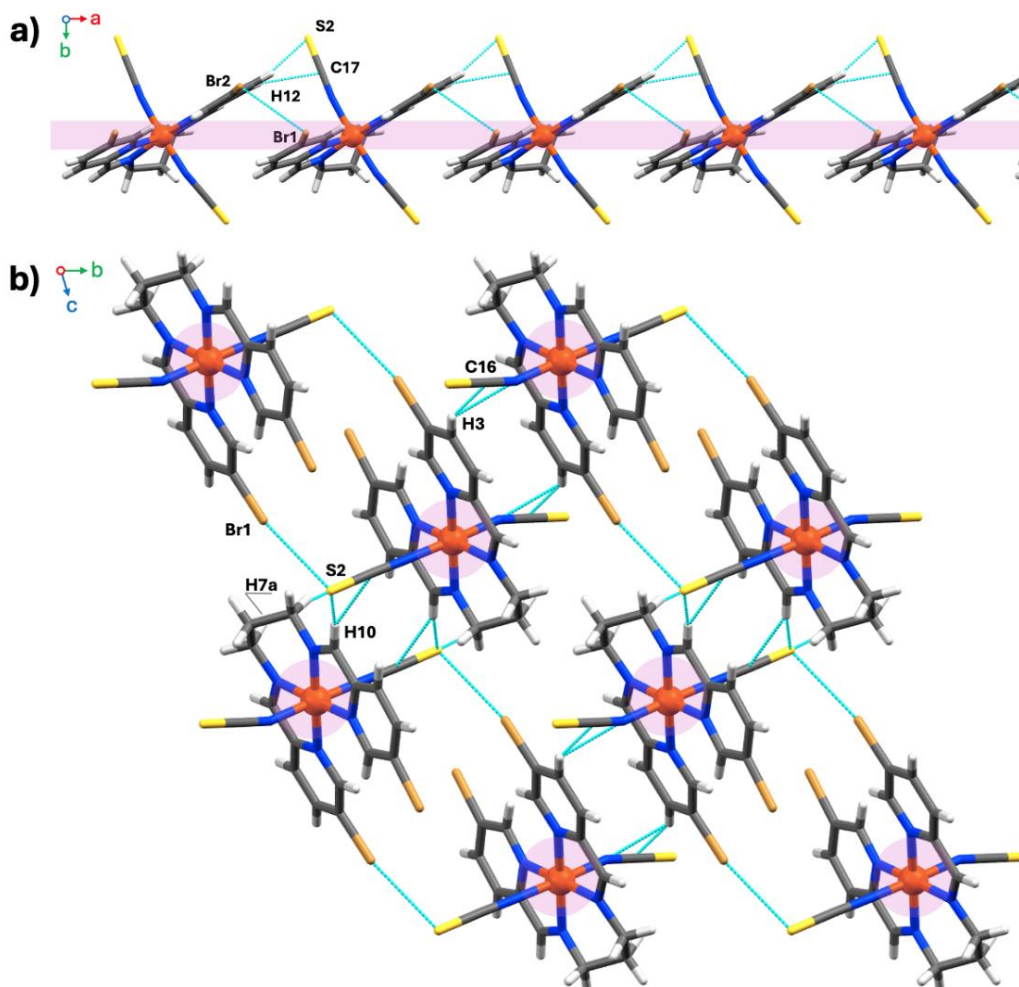*Figure S13: Packing interactions in polymorph B of [Fe(**L^{5Br-pyridine}**)(NCS)₂] **4B** at 100 K. a) View down the c-axis highlighting the formation of 1D supramolecular chains along the a-axis. Pink line to guide the eye. b) View down the a-axis highlighting the intermolecular interactions between the 1D chains described earlier. Pink dots to show the 1 D chains.*

*Table S8: Selected intermolecular contacts in the structure of **4B** at 100 K. All H atoms were inserted at calculated positions and rode on the attached non-H atom, with temperature factors U(H) = 1.2 U.*

D-H···A	H···A / Å	D···A / Å	D-H···A / °	Symm. Op for A	Figure
C7 – H7a ··· S2(NCS)	2.780	3.638(7)	148.0	2-x,1-y,-z	Fig. S13b
C10 – H10 ··· S2(NCS)	2.790	3.612(7)	149.0	1-x,1-y,-z	Fig. S13b
C12 – H12 ··· S2(NCS)	2.950	3.613(8)	130.0	-1+x,y,z	Fig. S13a
C12 – H12 ··· C17(NCS2)	2.830	3.481(10)	117.0	-1+x,y,z	Fig. S13a
C3 – H3 ··· C16(NCS1)	2.590	3.441(9)	152.0	2-x,-y,1-z	Fig. S13b
C3 – H3 ··· N5(NCS1)	2.706	3.382(9)	130.0		
Br1 ··· S2(NCS)		3.4278(19)		2-x,1-y,1-z	Fig. S13b
Br1 ··· Br2		3.6922(10)		1+x,y,z	Fig. S13a

*Figure S14: Photo of a single crystal of **4B** at 100 K.*

S2. Solid State Magnetic Data

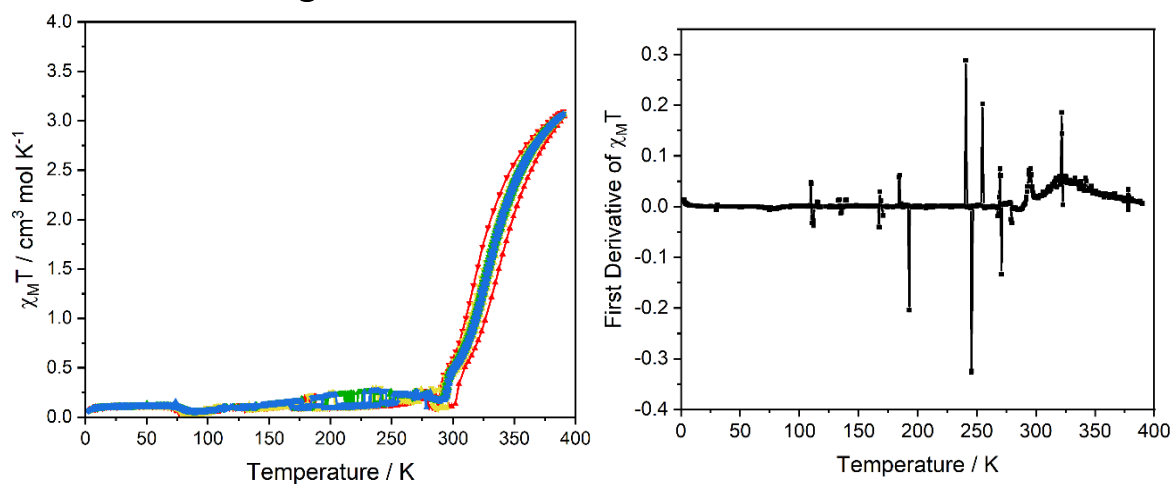*Figure S15: Left: Solid state magnetic measurements of **1** at varying scan rates (K min⁻¹): 10 (red), 5 (yellow), 2 (green), 1 (blue). Right: First derivative of the heating cycle of **1** measured at 1 K min⁻¹.*
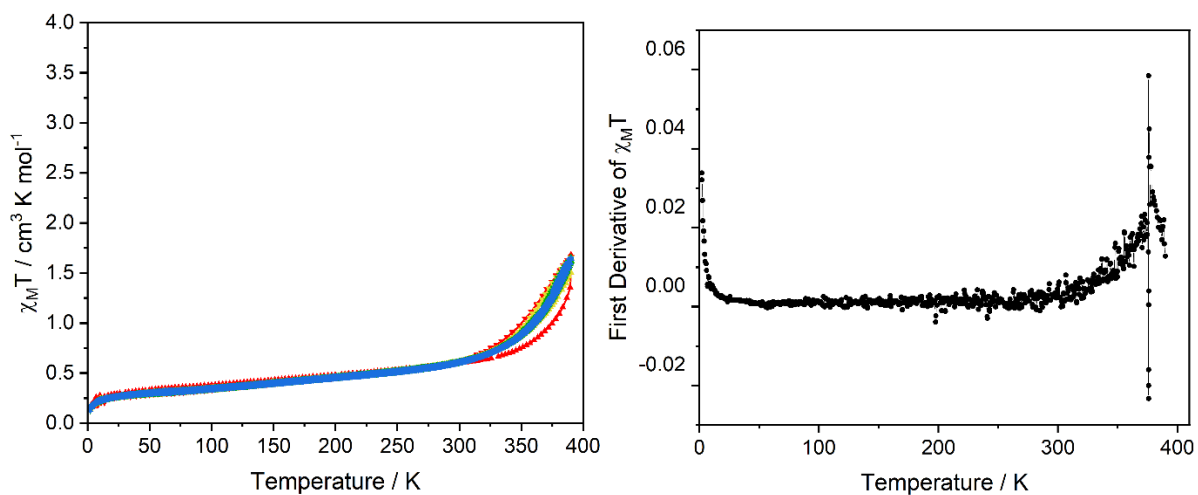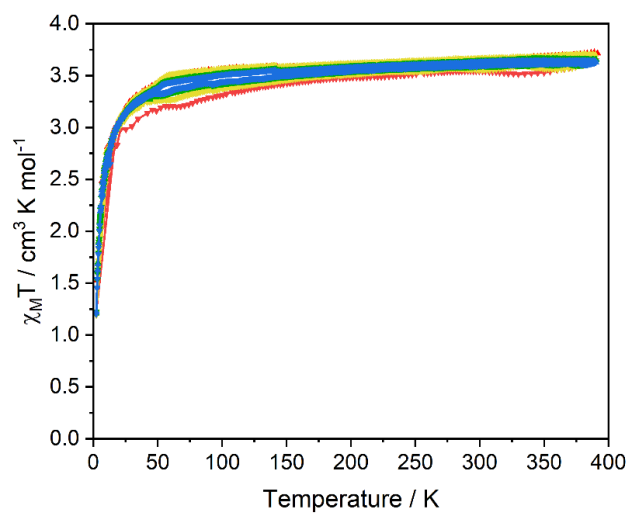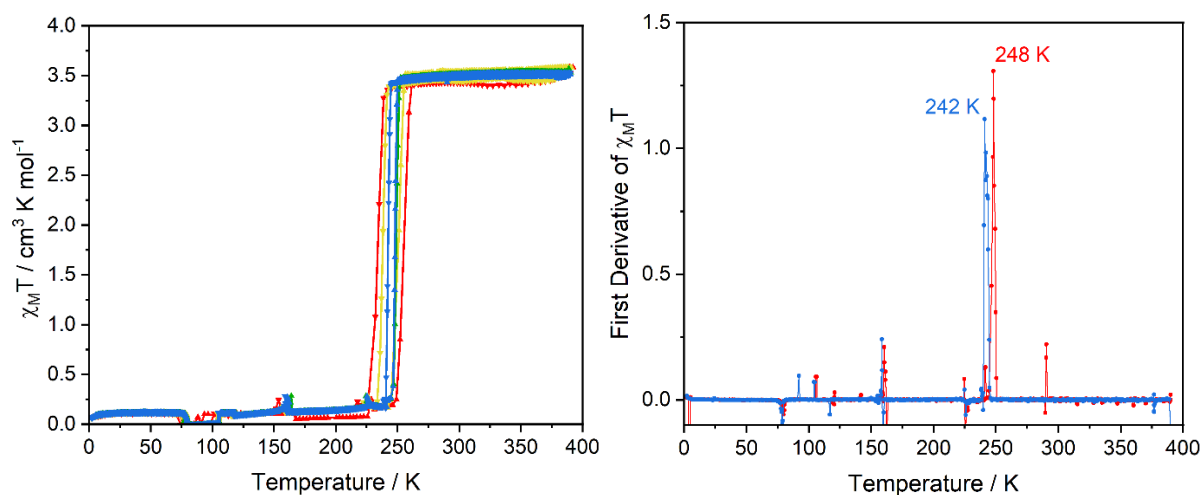

*Figure S16: Left: Solid state magnetic measurements of **2** at varying scan rates (K min⁻¹): 10 (red), 5 (yellow), 2 (green), 1 (blue). Right: First derivative of the heating cycle of **2** measured at 1 K min⁻¹.*

*Figure S17: Solid state magnetic measurements on **3** at varying scan rates (K min⁻¹): 10 (red), 5 (yellow), 2 (green), 1 (blue).*

*Figure S18: Left: Solid state magnetic measurements on **4A** at varying scan rates (K min⁻¹): 10 (red), 5 (yellow), 2 (green), 1 (blue). Right: First derivative of the heating cycle (red) and cooling cycle (blue) of **4A** measured at 1 K min⁻¹.*
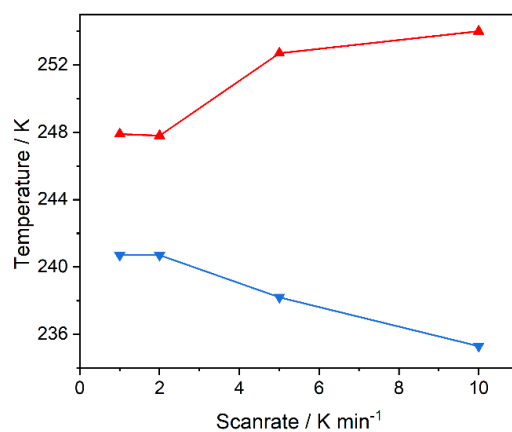

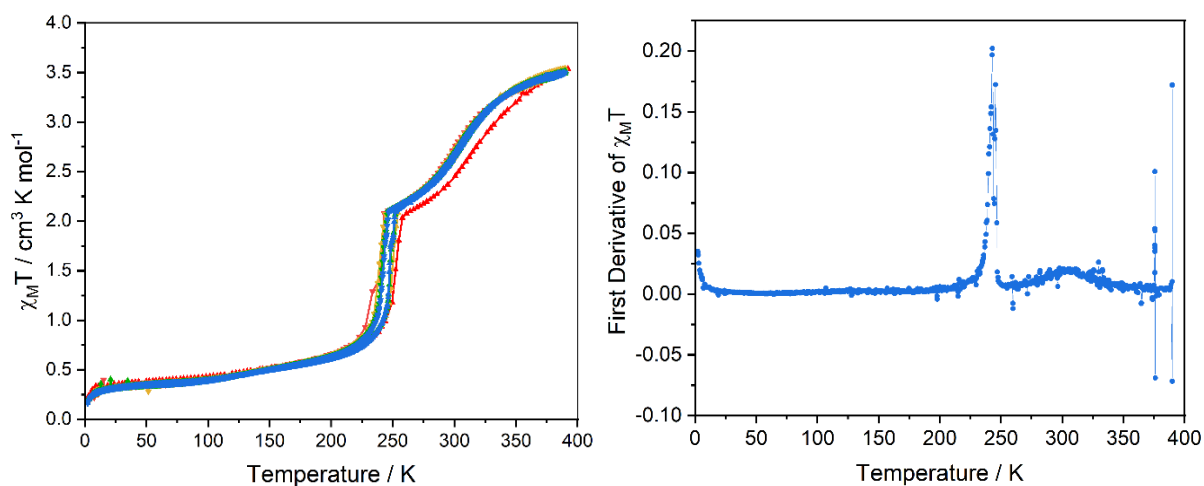*Figure S19: Plot of measured $T_{1/2}$ versus scanrate for **4A**.*

*Figure S20: Left: Solid state magnetic measurements of a mixture of **4A** and **4B** at varying scan rates (K min^{-1}): 10 (red), 5 (yellow), 2 (green), 1 (blue). Right: First derivative of the heating cycle of **4A** and **4B** measured at 1 K min^{-1}.*
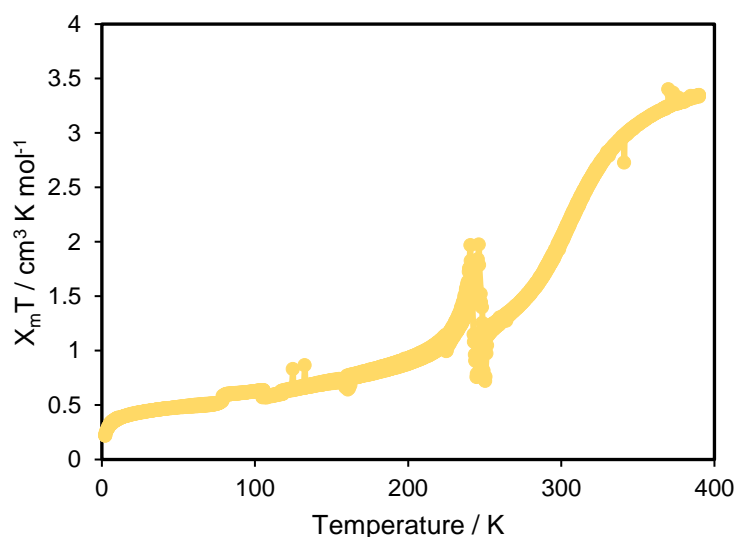

*Figure S21: Estimated solid state variable temperature magnetic data for **4B**, obtained by taking the data for the mixture **4A/4B** and subtracting **4A**, assuming 40% of the sample is **4A**. This assumption is based on the fact that the SCO curve for the mixture of **4A** and **4B** starts to deviate from the abrupt profile for **4A** to gradual profile for **4B** at about $\chi_M T(252 K) = 2.1$ cm^3 K mol^{-1}, eventually reaching a maximum of $\chi_M T(390 K) = 3.5$ cm^3 K mol^{-1}. This provides an estimated 2:3 ratio of **4A** to **4B** in the mixed sample, which in turn allows calculation of an estimated SCO plot for **4B** from these two datasets. Scan rate of 1 K min^{-1}.*

*Table S9: Determining the 'smoothness' of the spin transition for **1, 2** (not possible as doesn't reach 80% HS in the accessible T window), **4A** and **4B**. 'Smoothness' is defined as the difference in temperature between the sample at 20% HS, and 80% HS.[1]*

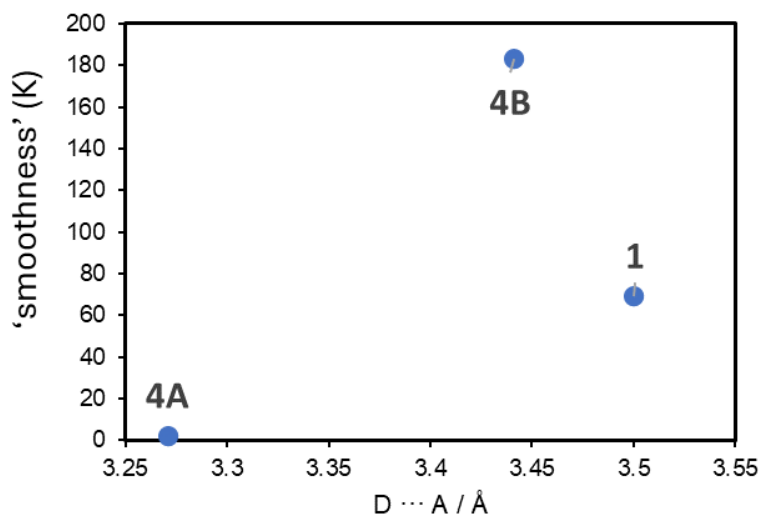|	1	2	4A	4B
20% HS	311	325	247	148
80% HS	380	-	249	331
Smoothness / K	69	N/A	2	183

*Figure S22: Plot of shortest intermolecular non-classical hydrogen bond C·· S(NCS) in each of these 3 complexes, versus the 'smoothness' of the spin transition (as defined above,[1] see Table S9). Complex **4A** has the smallest 'smoothness' value (hence the most abrupt SCO) and consistent with the literature expectation[1] also has the shortest C·· S(NCS). Added to this, **4A** undergoes a phase transition, which is also expected to enhance the abruptness of the SCO. As expected from the literature correlation,[1] the isomeric complex **4B** which has a higher 'smoothness' value (hence more gradual SCO) also features a longer 'shortest C·· S(NCS)'. Complex **1** does not fit the trend seen for the isomeric complexes **4A** and **4B**, but **1** features azoles not bromo-azines in the ligand.*

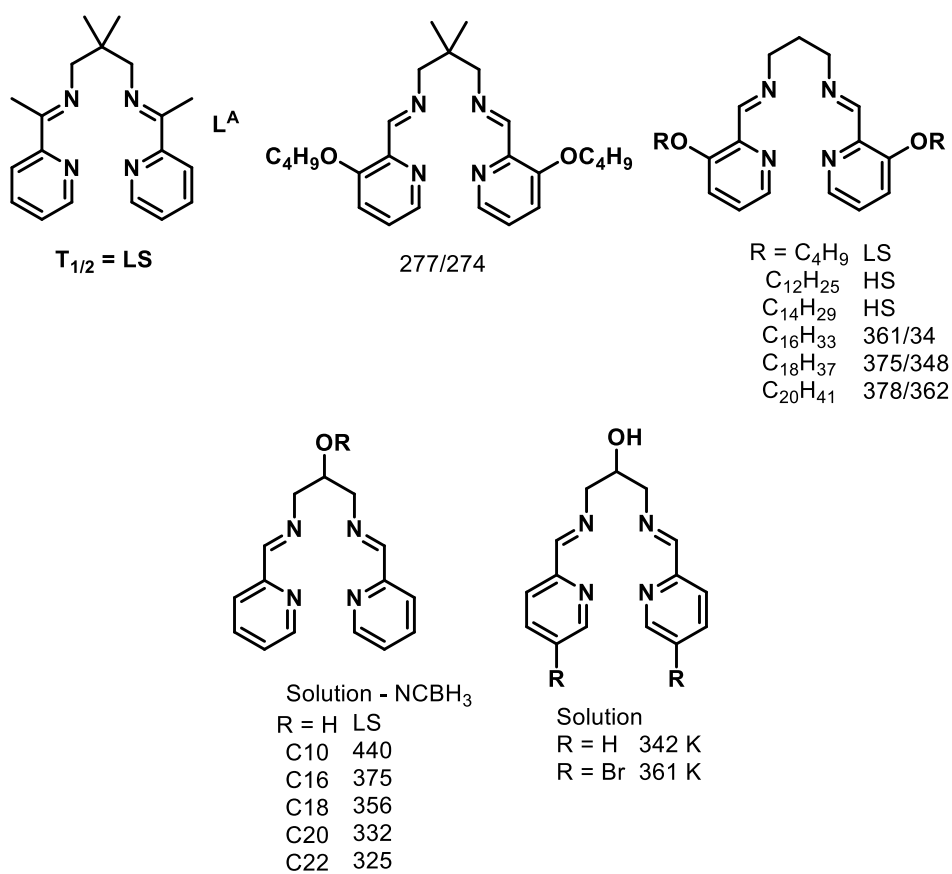# S3. Literature Tetradentate Schiff-Base Ligands and Fe(II) Complexes

Figure S23: Literature tetradentate ligands derived from one equivalent of 1,3-diaminopropane (and it's derivatives), and pyridyl-ketones/aldehydes. Grouped as **family A in Figure 1**. All $T_{1/2}$ values are reported for the [Fe(**L**)(NCS)$_2$] complex in the solid state unless otherwise noted. [2-5]

L^{B1}: R = H   HS
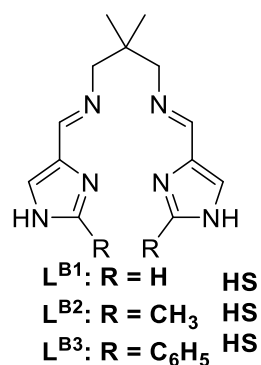L^{B2}: R = CH_3 HS
L^{B3}: R = C_6H_5 HS

*Figure S24: Literature tetradentate ligands derived from one equivalent of 1,3-diaminopropane (and it's derivatives), and two equivalent of a 2-R-1H-imidazol-4-aldehyde derivative. Grouped as **family B in Figure 1**. All T1/2 values are reported for the [Fe(L)(NCS)2] complex in the solid state.[5]*

Tup 409
Tdown 389

Tup 240
Tdown 239

.0.5H20
Tup 351 -> 335
Tdown 325 -> 310

.0.5MeCN.0.5MeO
H.H20
Tup 324 -> 322
Tdown 293 -> 285

Tup 259
Tdown 245
2 step

Tup 203
Tdown 187

Tup 224
Tdown 210

Tup 225
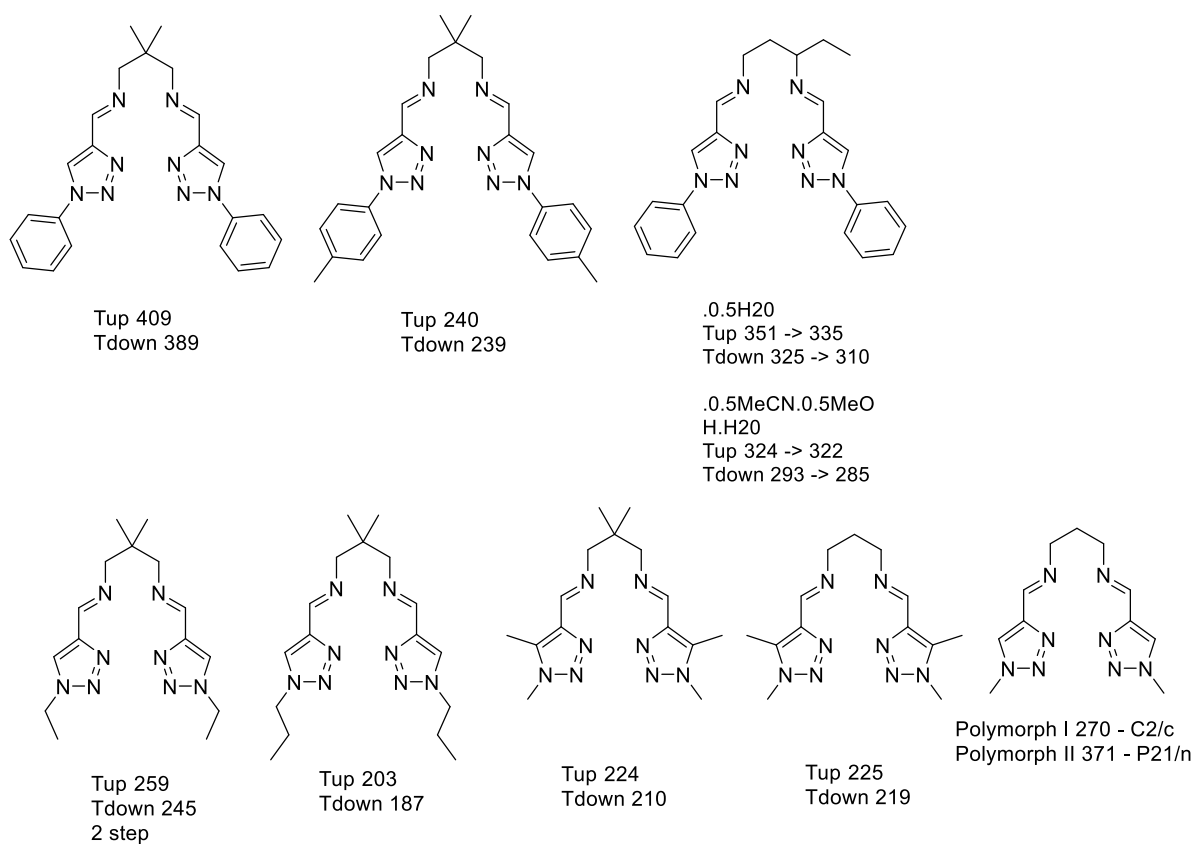Tdown 219

Polymorph I 270 - C2/c
Polymorph II 371 - P21/n

*Figure S25: Literature tetradentate ligands derived from one equivalent of 1,3-diaminopropane (and it's derivatives), and two equivalents of a 5-formyl-1,2,3-triazole derivative. Grouped as **family C in Figure 1**. All $T_{1/2}$ values are reported for the [Fe(**L**)(NCS)$_2$] complex in the solid state.[6, 7]*
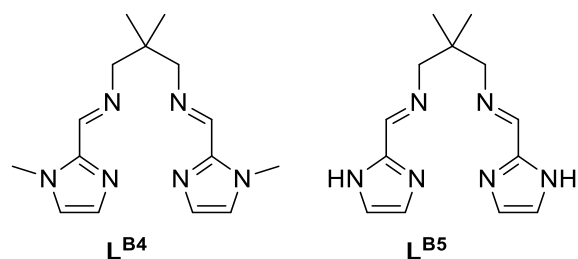

L^{B4} L^{B5}

*Figure S26: Literature tetradentate ligands derived from one equivalent of 1,3-diaminopropane (and it's derivatives), and two equivalenst of a 1-N-R-imidazol-2-carboxaldehyde derivative. Grouped as **family D in Figure 1**. All $T_{1/2}$ values are reported for the [Fe(**L**)(NCS)$_2$] complex in the solid state.[8]*
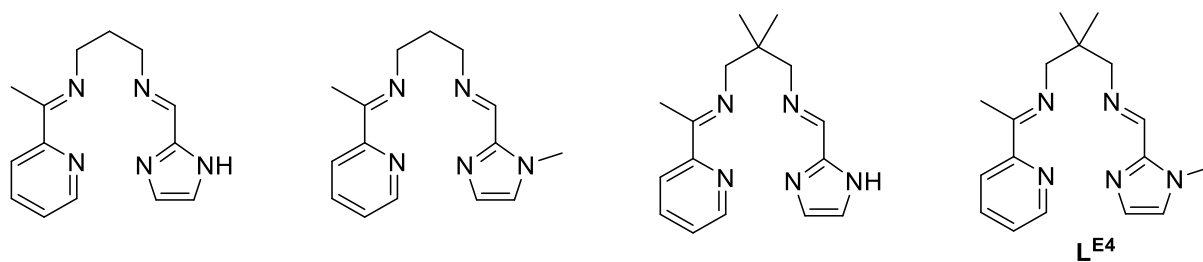
*Figure S27: Literature tetradentate ligands derived from one equivalent of 1,3-diaminopropane (and it's derivatives),), one equivalent of 2-acetylpyridine and one equivalent of a 1-N-R-imidazol-2-carboxaldehyde derivative. Grouped as **family E in Figure 1**. All $T_{1/2}$ values are reported for the [Fe(**L**)(NCS)$_2$] complex in the solid state.[8]*

L^{D1}
Dehydrated, T1 = 292
T2 = 202 (grad)

L^{D2}
T1/2 = 317
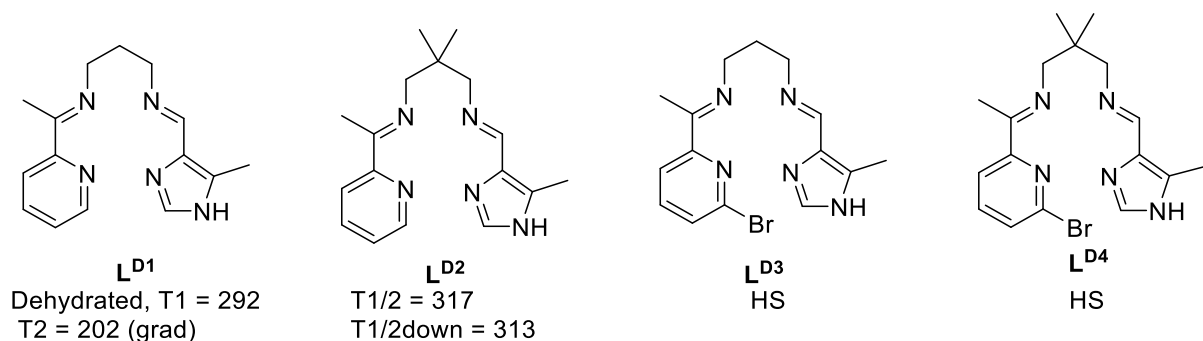T1/2down = 313

L^{D3}
HS

L^{D4}
HS

*Figure S28: Literature tetradentate ligands derived from one equivalent of 1,3-diaminopropane (and it's derivatives), one equivalent of 2-acetylpyridine and one equivalent of a 2-R-1H-imidazol-4-aldehyde derivative.. Grouped as **family F in Figure 1**. All $T_{1/2}$ values are reported for the [Fe(**L**)(NCS)$_2$] complex in the solid state.[9]*

L^{C1}: R = H   LS, 30%HS@400
L^{C2}: R = CH$_3$ HS
L^{C3}: R = C$_6$H$_5$ Mostly HS

L^{C4}: R = H   LS, 30%HS@400
L^{C5}: R = CH$_3$ HS
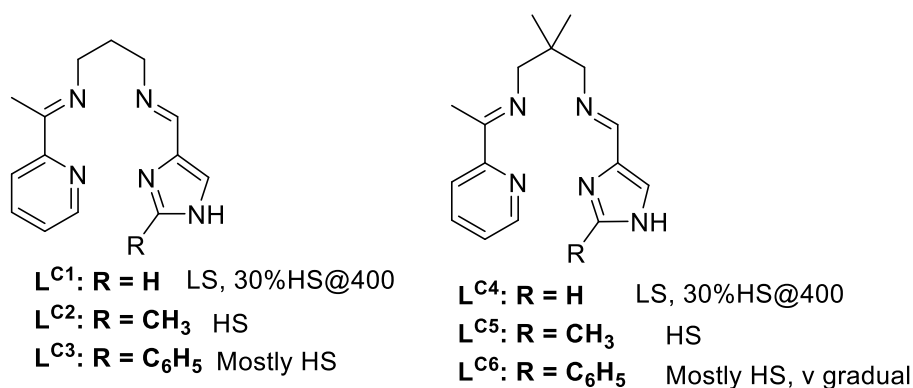**L^{C6}: R = C$_6$H$_5$**   Mostly HS, v gradual

*Figure S29: Literature tetradentate ligands derived from one equivalent of 1,3-diaminopropane (and it's derivatives), one equivalent of 2-acetylpyridine and one equivalent of a 2-R-1H-imidazol-4-aldehyde. Grouped as **family F in Figure 1**. All $T_{1/2}$ values are reported for the [Fe(**L**)(NCS)$_2$] complex in the solid state.[5]*

S4. References

1.   P. Guionneau, M. Marchivie, G. Bravic, J.-F. Létard and D. Chasseau, *Top. Curr. Chem.*, 2004, **234**, 97-128.

2.   S. Sundaresan, J. A. Kitchen and S. Brooker, *Inorg. Chem. Front.*, 2020, **7**, 2050–2059.

3.   S. Sundaresan and S. Brooker, *Inorg. Chem.*, 2023, **62**, 12192-12202.

4.   M. Seredyuk, K. Znovjyak, M. C. Munoz, Y. Galyametdinov, I. O. Fritsky and J. A. Real, *RSC Adv.*, 2016, **6**, 39627-39635.

5.   N. Bréfuel, I. Vang, S. Shova, F. Dahan, J.-P. Costes and J.-P. Tuchagues, *Polyhedron*, 2007, **26**, 1745-1757.

6.   M. Seredyuk, K. Znovjyak, F. J. Valverde-Muñoz, M. C. Muñoz, V. M. Amirkhanov, I. O. Fritsky and J. A. Real, *Inorg. Chem.*, 2023, **62**, 9044-9053.

7.   H. Hagiwara, T. Masuda, T. Ohno, M. Suzuki, T. Udagawa and K.-i. Murai, *Cryst. Growth Des.*, 2017, **17**, 6006-6019.

8.   N. Bréfuel, S. Shova and J.-P. Tuchagues, *Eur. J. Inorg. Chem.*, 2007, 4326-4334.

9.   N. Bréfuel, S. Shova, J. Lipkowski and J.-P. Tuchagues, *Chem. Mater.*, 2006, **18**, 5467-5479.